The Energy Dispersion of the Chain Band in $YBa_2Cu_3O_{6+y}$ and Its Effect on the Cu(2) NQR Frequency *

M. V. Eremin and R. Markendorf
Physik-Institut, Universität Zürich, Zürich, Switzerland

and S. G. Solovjanov
Physics Department, Kazan State University, 420008, Russia

Z. Naturforsch. **49a**, 379–384 (1994); received September 7, 1993

The energy dispersion of the chain band has been determined in the framework of the Hubbard model. The results are in agreement along the Γ–S and Γ–Y lines of the Brillouin zone with photoemission data. The amount of $d_{3z^2-r^2}$ states is zero at $y=0$ and increases to 10% at $y=1$. The admixture is due to the hybridization of Cu(1) $d_{y^2-z^2}$ states with Cu(2) $d_{3z^2-r^2}$ states via apical oxygen. The effect of this admixture on the NQR frequency of Cu(2) is discussed.

Key words: NQR, Electron correlation, Chain band, $d_{3z^2-r^2}$ states, Band dispersion.

I. Introduction

Our calculations were stimulated by the following experimental data. According to photoemission studies ([1] and references therein) a considerable amount of states with $d_{3z^2-r^2}$ symmetry resides near the Fermi level. The reason for that has not been quite clarified yet. The amount of $d_{3z^2-r^2}$ allows for an explanation of the NQR frequency of Cu(2) [2]. High-resolution photoemission measurements are reported for $YBa_2Cu_3O_{6+y}$ [3]. Two bands intersecting the Fermi energy on the Γ–S line were observed. In contrast to the prediction of the usual band theory the observed dispersion is small. One of the reasons for that is that usual band theory fails for systems with strong electron correlation. In high-temperature superconductors (HTSC) the intra-atomic interactions of copper and oxygen states are very strong with respect to usual metals, and therefore the Hubbard model provides the proper theoretical background.

This paper is organized as follows. First, we present a Hubbard-like Hamiltonian for a model which contains two planes and one chain per unit cell and thus the main electronic charge transfers. The energy spectrum is determined with the help of Greens functions. The equations of motion are determined in the Hubbard-I approximation and are solved numerically. The resulting bands are compared with photoemission data. Finally we compare with experimental data, namely with the doping dependence of the NQR frequency.

II. Model Hamiltonian and Energy Spectrum

The orbitals, which are taken into account, are shown in Figure 1. Figure 1 a represents the undoped case with no holes in the chain. Oxygen doping introduces holes into the chain and plane orbitals of Fig. 1 b, allowing for a hybridization between them. The whole Hamiltonian is then given by

$$H = H^{(1)}_{\text{plane}} + H^{(2)}_{\text{plane}} + H_{\text{chain}} + V_{\text{int}} \,. \tag{1}$$

V_{int} describes the hopping of holes between planes and chain via the apical oxygen. The plane Hamiltonian reads

$$\begin{aligned} H = {} & \varepsilon_\varepsilon \sum_{i\sigma} X_i^{\sigma,\sigma} + \varepsilon_\theta \sum_{i\sigma} Y_i^{\sigma,\sigma} + \varepsilon_p \sum_{j\sigma} p_j^{\sigma,\sigma} \\ & + \sum_{ij} t_{ij}^{p\varepsilon} (X_i^{\sigma,0}\, p_j^{0,\sigma} + p_j^{\sigma,0}\, X_i^{0,\sigma}) \\ & + \sum_{ij} t_{ij}^{p\theta} (Y_i^{\sigma,0}\, p_j^{0,\sigma} + p_j^{\sigma,0}\, Y_i^{0,\sigma}) + \sum_{jj'} t_{jj'}^{pp}\, p_j^{\sigma,0}\, p_{j'}^{0,\sigma} \\ & + (V_{pd} - K_{pd}) \sum_i \psi_i^+ \psi_i \,. \end{aligned} \tag{2}$$

* Presented at the XIIth International Symposium on Nuclear Quadrupole Resonance, Zürich, July 19–23, 1993.

Reprint requests to R. Markendorf, Physik-Institut, Universität Zürich, Winterthurerstr. 190, CH-8057 Zürich, Switzerland.

0932-0784 / 94 / 0100-0379 $ 01.30/0. – Please order a reprint rather than making your own copy.

Here $X^{\sigma\sigma'}$ and $Y^{\sigma\sigma'}$ are Hubbard operators for $|\varepsilon\rangle = |x^2-y^2\rangle$ and $|\Theta\rangle = |3z^2-r^2\rangle$ copper states, $p_j^{\sigma\,0}$ is the hole creation operator for oxygen in the lower Hubbard band and ψ_i^+ is the creation operator for Zhang-Rice singlet states of copper and oxygen holes [4]

$$\psi_i = \frac{1}{\sqrt{2}} (P_{i\uparrow} X_i^{0\downarrow} - P_{i\downarrow} X_i^{0\uparrow}) . \tag{3}$$

The linear combination $P_{i\sigma}$ of the four p_σ oxygen hole states around a copper hole $|d_{x^2-y^2}\rangle$ state is

$$P_{i\sigma} = \tfrac{1}{2} (p_i^{(1)\,0,\sigma} - p_i^{(2)\,0,\sigma} - p_i^{(3)\,0,\sigma} + p_i^{(4)\,0,\sigma}) . \tag{4}$$

The expression for K_{pd} is given by

$$K_{pd} = t_\sigma^2 \left[\frac{6}{U_{dd} - \Delta_1 - 2V_{pd}} + \frac{1.5}{U_{pp} + \Delta_1} \right] . \tag{5}$$

It is caused by the virtual exchange via the upper copper and oxygen Hubbard bands only. All parameters needed for our model were already discussed in [5, 6]. Δ_1 is the charge transfer gap of about 2 eV. The Coulomb repulsion of holes at the copper and oxygen site amounts to $U_{dd} \sim 9$ eV and $U_{pp} \sim 6$ eV, respectively. The terms in (5) occur in accord with those of Matsukawa and Fukuyama [6], because we took into account the exchange interaction of the copper ground state $|x^2-y^2\rangle$ with the excited copper state $|x^2-y^2\rangle$, which in turn hybridizes with the oxygen p_σ orbitals too. $U_{dd'}$ is an effective repulsion energy of holes in $|x^2-y^2\rangle$ and $|3z^2-r^2\rangle$ states, which is about 8 eV. Δ_2 is the charge transfer energy from oxygen to excited copper states $|3z^2-r^2\rangle$. Its value is about 3 eV [6]. With these values K_{pd} is according to (5) about 2.3 eV. Furthermore we use according to [5, 6] and references therein the following parameters: $V_{pd} = 1$ eV, charge transfer energy from the oxygen to the $|x^2-y^2\rangle$ copper state $\varepsilon_p - \varepsilon_\varepsilon = 2$ eV, copper-oxygen transfer integral $t_0 = 1.2$ eV, transfer integral between the nearest oxygen atoms $t_{xy}^{pp} = t_{xz}^{pp} = t_{yz}^{pp} = 0.6$ eV and between the next nearest oxygen neighbours $t_{xx}^{pp} = t_{yy}^{pp} = t_{zz}^{pp} = 0.4$ eV. The axial copper orbital $|3z^2-r^2\rangle$ lies $\varepsilon_\Theta - \varepsilon_\varepsilon = 1$ eV above the planar copper orbital, and the energy $\varepsilon_d^{Cu(1)}$ of the chain $|y^2-z^2\rangle$ copper orbitals lies 0.8 eV above ε_ε.

This model leads to a 12 × 12 eigenvalue equation, which is constructed employing the Greens function method. The coupled equations of motion are terminated by the Hubbard-I approximation. For the matrix $\boldsymbol{a} = a_{ij}$ of the eigenvalue equation

$$|\, \boldsymbol{a} - \boldsymbol{I}E| = 0 \tag{6}$$

we obtain

$$\boldsymbol{a} = \begin{pmatrix}
\varepsilon_\varepsilon & 0 & -i\sqrt{3}P_\varepsilon t_k^x & i\sqrt{3}P_\varepsilon t_k^y & 0 & 0 & \dots \\
0 & \varepsilon_\Theta & iP_\Theta t_k^x & iP_\Theta t_k^y & P_\Theta t_\sigma e^{-ik_z c} & 0 & \dots \\
i\sqrt{3}P_p t_k^x & -iP_p t_k^x & \varepsilon_{pk}^x & P_p t_k^{xy} & iP_p t_k^{xz} e^{-ik_z c} & 0 & \dots \\
-i\sqrt{3}P_p t_x^y & -iP_p t_k^y & P_p t_k^{xy} & \varepsilon_{pk}^y & iP_p t_k^{yz} e^{-ik_z c} & 0 & \dots \\
0 & P_p' t_\sigma e^{ik_z c} & -iP_p' t_k^{xz} e^{ik_z c} & -iP_p' t_k^{yz} e^{ik_z c} & \varepsilon_p^{(4)} & -\frac{\sqrt{3}}{2} P_p' t_\sigma e^{-ik_z c} & \dots \\
0 & 0 & 0 & 0 & -\frac{\sqrt{3}}{2} t_\sigma P_d' e^{ik_z c} & \varepsilon_d^{Cu(1)} & \dots \\
0 & 0 & 0 & 0 & -iP_p' t_k^{yz} e^{ik_z c} & -i\sqrt{3}P_p' t_k^y & \dots \\
0 & 0 & 0 & 0 & P_p' t^{zz} e^{2ik_z c} & -\frac{\sqrt{3}}{2} P_p' t_\sigma e^{ik_z c} & \dots \\
0 & 0 & 0 & 0 & 0 & 0 & \dots \\
0 & 0 & 0 & 0 & 0 & 0 & \dots \\
0 & 0 & 0 & 0 & 0 & 0 & \dots \\
0 & 0 & 0 & 0 & 0 & 0 & \dots
\end{pmatrix}$$

where we used the abbreviations

$$t_k^x = t_\sigma \sin\frac{k_x a}{2}, \quad t_k^y = t_\sigma \sin\frac{k_y a}{2}, \tag{8}$$

$$t_k^{xx} = 2t_{xx}^{pp}\cos k_x a, \quad t_k^{yy} = 2t_{yy}^{pp}\cos k_y a, \tag{9}$$

$$t_k^{xy} = 4t_{xy}^{pp}\sin\frac{k_x a}{2}\sin\frac{k_y a}{2}, \tag{10}$$

$$t_k^{xz} = 2t_{xz}^{pp}\sin\frac{k_x a}{2}, \quad t_k^{yz} = 2t_{yz}^{pp}\sin\frac{k_y a}{2}, \tag{11}$$

$$t^{zz} = t_{zz}^{pp}, \tag{12}$$

$$\varepsilon_{pk}^x = \varepsilon_p - P_p t_k^{xx}, \quad \varepsilon_{pk}^y = \varepsilon_p - P_p t_k^{yy}, \tag{13}$$

$$\varepsilon_{pk}^{y'} = \varepsilon_p' - P_p' t_k^{yy} \tag{14}$$

for the transfer integrals and diagonal terms. $\varepsilon_d^{Cu(1)}$ is the energy level of the chain $|y^2 - z^2\rangle$ state, ε_p are the energies of p_x and p_y in the chain and $\varepsilon_p^{(4)}$ that of the p'_z state of the apical oxygen. The Hubbard reduction factors P are the thermodynamic averages over the anticommutators of the corresponding hole operators. For short we present here only the final values for $YBa_2Cu_3O_7$:

$$P_\varepsilon = 0.6, \quad P_\Theta = 0.9, \quad P_p = 0.875,$$
$$P_d' = 0.7, \quad P_p' = 0.85. \tag{15}$$

A prime in P_p' and P_d' denotes always Hubbard reductions for the related chain bands, where mainly the $|y^2 - z^2\rangle$ and the p_y' states enter. In particular P_p' refers also to the apical oxygen p_z' orbital.

Figure 1 shows the 12 orbitals which are included here. The planar $|x^2 - y^2\rangle$ and $|p_x\rangle$, $|p_y\rangle$ orbitals in Fig. 1 a determine the plane bands. The chain band is governed by the orbitals $|y^2 - z^2\rangle$ and p_y', which are shown in the middle part of Fig. 1 b. Additionally the hybridization between $|y^2 - z^2\rangle$ and the axial plane orbital $|3z^2 - r^2\rangle$ via the apical oxygen p_z state mixes a small amount of $|3z^2 - r^2\rangle$ into the chain band. This electronic path is also sketched in Figure 1 b.

Figure 2 shows the numerical solution of (6) and (7) for $k_z = 0$ along the diagonal of the Brillouin zone and along the k_y axis. Bands I and II are the lower antibonding Hubbard bands which have mainly $|x^2 - y^2\rangle$ character. The full dispersion of bands I is represented in Figure 3. In the antiferromagnetic isolator these bands are completely occupied. Band III is the $|y^2 - z^2\rangle$ chain band dispersing through the Fermi energy in $YBa_2Cu_3O_{6+y}$ at high enough doping $y \geq 0.4$. The two bands IV and V are the axial $|3z^2 - r^2\rangle$ plane bands, followed by the nonbonding (two-fold degenerated) and bonding oxygen bands VI and VII. We mention that a second band, due to the Zhang-Rice singlet states in the last term in (2), crosses the Fermi energy. We omitted it in Fig. 2 for the sake of clearness and because only knowledge of its existence rather than its details is necessary for discussing the NQR frequency. The details are given in [7]. For our present purpose we state that the oxygen holes,

$$\begin{vmatrix}
\dots & 0 & 0 & 0 & 0 & 0 & 0 \\
\dots & 0 & 0 & 0 & 0 & 0 & 0 \\
\dots & 0 & 0 & 0 & 0 & 0 & 0 \\
\dots & 0 & 0 & 0 & 0 & 0 & 0 \\
\dots & iP_p' t_k^{yz} e^{-ik_z c} & P_p' t^{zz} e^{-i2k_z c} & 0 & 0 & 0 & 0 \\
\dots & i\sqrt{3}P_d' t_k^y & -\frac{\sqrt{3}}{2} P_d' t_\sigma e^{-ik_z c} & 0 & 0 & 0 & 0 \\
\dots & \varepsilon_{pk}^{y'} & -iP_p' t_k^{yz} e^{-ik_z c} & 0 & 0 & 0 & 0 \\
\dots & iP_p' t_k^{yz} e^{ik_z c} & \varepsilon_p^{(4)} & -iP_p' t_k^{yz} e^{-ik_z c} & -iP_p' t_k^{xz} e^{-ik_z c} & P_p' t_\sigma e^{-ik_z c} & 0 \\
\dots & 0 & iP_p' t_k^{yz} e^{ik_z c} & \varepsilon_{pk}^y & P_p t_k^{xy} & -iP_p t_k^y & -i\sqrt{3}P_p t_k^y \\
\dots & 0 & iP_p t_k^{xz} e^{ik_z c} & P_p t_k^{xy} & \varepsilon_{pk}^x & -iP_p t_k^x & i\sqrt{3}P_p t_k^x \\
\dots & 0 & P_\Theta t_\sigma e^{ik_z c} & iP_\Theta t_k^y & iP_\Theta t_k^x & \varepsilon_\Theta & 0 \\
\dots & 0 & 0 & i\sqrt{3}P_\varepsilon t_k^y & -i\sqrt{3}P_\varepsilon t_k^x & 0 & \varepsilon_\varepsilon
\end{vmatrix} \tag{7}$$

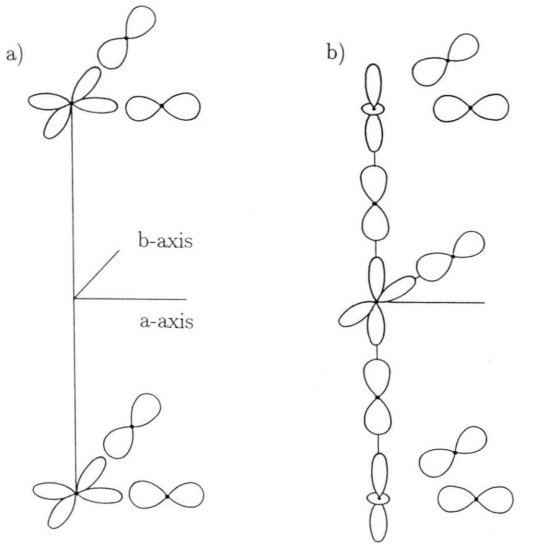

Fig. 1. Schematic picture of orbitals which are (partially) occupied with holes in the undoped case (a) and after doping with oxygen (b).

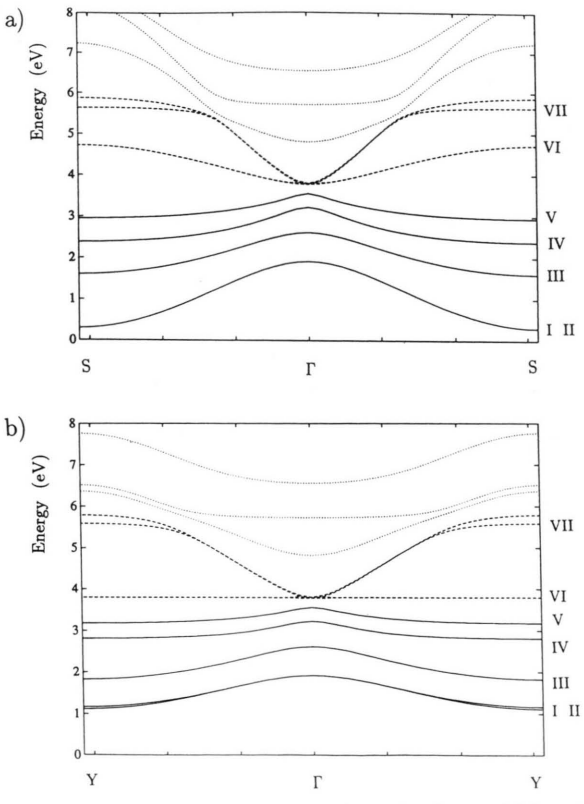

Fig. 2. Calculated enery spectrum along the diagonal (a) and along the k_y axis (b), representing bands with mainly copper (——), mainly planar oxygen (– – –) and mainly chain and apical oxygen (· · · · ·) character.

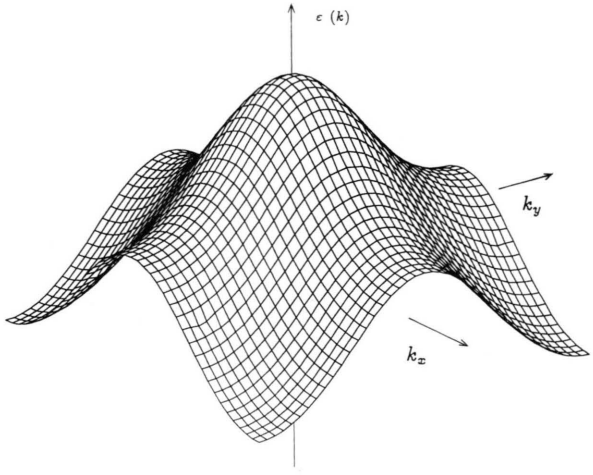

Fig. 3. Energy dispersion for the lower Hubbard band I in Fig. 2 in the whole Brillouin zone.

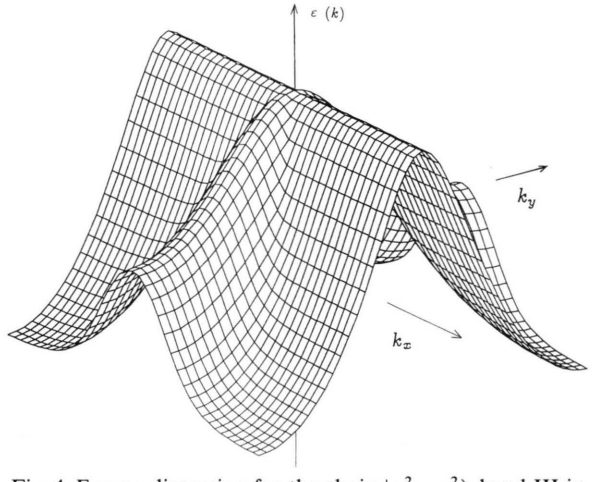

Fig. 4. Energy dispersion for the chain $|y^2 - z^2\rangle$ band III in Fig. 2 in the whole Brillouin zone.

which are responsible for the reduced lattice contribution (16) at increased doping, reside in this band (see section III).

The bands near E_F have recently been studied by Liu et al. through angle-resolved photoemission [3]. For comparison the dispersion of the chain band III in the whole Brillouin zone is given in Figure 4. It shows the right behavior along the diagonal and the k_x and k_y axis. According to Liu et al. the chain band has a strong dispersion along the Γ–S diagonal, where it intersects E_F. A weaker dispersion was found by them along the lines Γ–X and Γ–Y in agreement with Figure 4. For a numerical comparison the chain

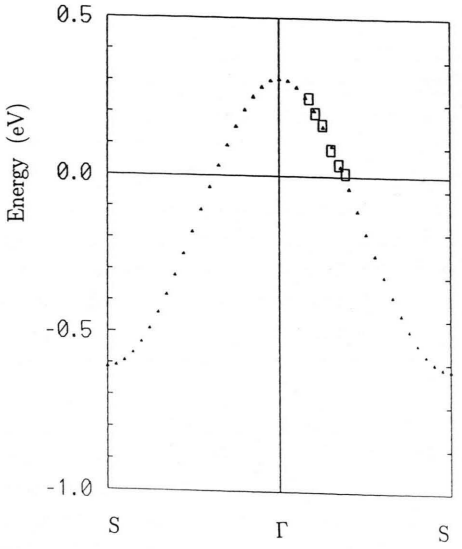

Fig. 5. Energy dispersion of the chain band in comparison with photoemission data (□).

band was drawn in Fig. 5 along the diagonal together with photoemission data [3] for $y = 0.9$ using the hole picture. The agreement is excellent. The second band that Liu et al. found to cross at E_F is attributed to the singlet correlated band [7].

III. The Electric Field Gradient at Cu(2)

There are four important contributions to the electric field gradient (EFG) at Cu(2). The EFG from the effective charges of the lattice is given by [2]

$$q_1 = (1-\gamma_\infty)\sum_j \frac{q_j}{R_j^3}(3z_j^2 - R_j^2), \tag{16}$$

where γ_∞ is the antishielding factor [8]. The gradient produced by the $|\varepsilon\rangle = |x^2-y^2\rangle$ and $|\Theta\rangle = |3z^2-r^2\rangle$ copper states has the form [2]

$$q_2 = -\frac{4}{7}\left\langle\frac{1}{r^3}\right\rangle_{3d}(n_\varepsilon - n_\Theta)(1-R_d), \tag{17}$$

where n_ε and n_Θ are the numbers of copper holes in the related states and R_d is the R-antishielding factor. The term due to the asymmetric overlap of the 3p copper core states with the 2p oxygen states can be written as [9]

$$q_3 = \frac{16}{5}\left\langle\frac{1}{r^3}\right\rangle_{3p}(S_{3p\sigma}^2 + S_{3ps}^2 + S_{3p\pi}^2). \tag{18}$$

The fourth contribution stems from the asymmetric overlap of the 3d copper with the 2p, 2s oxygen states and virtual charge transfer processes [10]

$$p_4 = \frac{4}{7}\left\langle\frac{1}{r^3}\right\rangle_{3d}[3(\gamma_{3d\sigma}+2S_{3d\sigma})\gamma_{3d\sigma} - \tfrac{2}{5}S_{3d\pi}^2 - 3S_{3d\pi}^2 - 3S_{3ds}^2 + \tfrac{2}{5}\gamma_{3d\pi}(\gamma_{3d\pi}+2S_{3d\pi})]. \tag{19}$$

Here $\gamma_{3d\sigma}$ and $\gamma_{3d\pi}$ are the so-called covalence parameters. These contributions were evaluated for $YBa_2Cu_3O_6$ using Hartree-Fock wave functions of Cu^{2+} and O^{2-} for the expectation values $\left\langle\frac{1}{r^3}\right\rangle$ and the hybridization terms [10], yielding the following values in MHz

$$q_1 = 30.5,\ q_2 = -97.3,\ q_3 = 16.4,\ q_4 = 28.5. \tag{20}$$

The NQR frequency of Cu(2) in $YBa_2Cu_3O_{6+y}$ is considerably influenced by the number of holes. It is 22.4 MHz at $y = 0$ and 31.3 MHz at $y = 1$ [11]. In our model the number of $|3z^2-r^2\rangle$ holes in the chain band is zero at $y = 0$ and increases up to 10% at $y = 1$. The admixture is due to hybridization of Cu(1) $|y^2-z^2\rangle$ states with Cu(2) $|3z^2-r^2\rangle$ states via the apical oxygen, see Fig. 1 b. The EFG's in $YBa_2Cu_3O_{6+y}$ were calculated by Schwarz et al. using their full-potential linear augmented-plane-wave model within the local-density approximation (LDA) [12, 13]. Here we use the hole picture for a discussion of their results in connection with ours. Schwarz et al. find rather good agreement of the theoretical EFG's with the experiment at nearly all sites, except of Cu(2). They state that the number of holes in the $|3z^2-r^2\rangle$ orbital was overestimated by their calculations [12]. This is probably due to LDA, because further inclusion of correlation effects would lead to narrower bands. For the given band structure that would lead to a smaller hole occupation in the $|3z^2-r^2\rangle$ state. To make their results agree with experiment a transfer of 0.07 holes from $|3z^2-r^2\rangle$ to $|x^2-y^2\rangle$ states would be needed in the case of $YBa_2Cu_3O_7$. That would lead to an axial hole occupation inside the copper sphere of about 0.04 [14]. This occupation number is already lower than our value. On the other hand the number of $|x^2-y^2\rangle$ holes, which are affected most by correlation, is considerably lower in [12] than our value of about 0.8.

The comparison of [12, 13] with our results shows that, refering to LDA, additional inclusion of many-particle correlation hould deplete the number of holes with $|3z^2-r^2\rangle$ symmetry (fills these states with electrons) and increases the number of $|x^2-y^2\rangle$ holes (empties these electronic states). This trend is also sup-

ported by comparing the results of [12] with experiment. In this respect first principles EFG calculations that go beyond LDA are of interest.

On the other hand, the slight tendency in [12] that doping enhances the axial Cu(2) hole occupation is much more pronounced in our calculations. From (17) and (20) one would expect a decrease of the EFG with doping, in contrast to experiment [11]. This may be explained by the fact that the doping reduces the effective charge of the oxygen ions near Cu(2), leading to a strong decrease of the lattice contribution (16), which has the opposite sign to (17). It is known from various experiments that holes go mainly into the oxygen orbitals. So there is considerable evidence that the lattice contribution (16) falls more strongly with doping than the amount of the local valence contribution (17) but both together result in a growing EFG. This is also consistent with the idea [15], that the Cu(2) NQR signal corresponds only to oxygen enriched regions in the plane.

IV. Conclusion

We have shown that the Hubbard model provides an accurate description of the energy dispersion of the chain band in $YBa_2Cu_3O_{6+y}$. The band width gets narrower than that of the usual band theory due to the many-particle band renormalization factors P in the Hubbard model. The band behavior along the main symmetry lines is in qualitative agreement with measurements by Liu et al. [3], especially with respect to the dispersion of the broader band crossing E_F. Moreover there is quantitative agreement with [3] along the $\Gamma-S$ line. Indeed, according to Bucher et al. [16] the resistivity parallel to the b-axis ϱ_b in $YBa_2Cu_4O_8$ originates mainly from the conduction channel with chain character and manifests predominantly a Bloch-Grüneisen form for metallic chains in distinct contrast to ϱ_a, which to our opinion is dominated by the second band, found by Liu et al. Here we mention only that this resistivity anisotropy of the chain contribution may be well understood using our dispersion as presented in Figure 4. The second (narrower) band passing through E_F, that was experimentally determined by Liu et al., is attributed to a singlet correlated impurity band. It is related to Zhang-Rice singlets [4] and has a dispersion [7] as observed experimentally [3].

Concerning the EFG at Cu(2) we have considered some trends. The EFG at Cu(2) is sensitive to the occupation of the axial $|3z^2-r^2\rangle$ and planar $|x^2-y^2\rangle$ copper orbitals, see (17). A comparison of our calculations with those by Schwarz et al. [12] shows that our correlation treatment has the tendency to lower the $|3z^2-r^2\rangle$ hole occupation and to increase the $|x^2-y^2\rangle$ hole occupation.

The $|3z^2-r^2\rangle$ orbitals enter the $|y^2-z^2\rangle$ chain band by hybridization via the apical oxygen. An analysis of the valence and the lattice contributions to the EFG show that at increased doping, the leading effect on the change of the Cu(2) EFG comes from the lattice contribution (16) and a minor influence comes from the raise of the $|3z^2-r^2\rangle$ hole occupation, reducing slightly the amount of the total valence term (17).

Acknowledgements

The authors acknowledge valuable discussions with Prof. K. Schwarz. Thanks are also due to Prof. D. Brinkmann, Dr. M. Mali, and Dr. J. Roos for numerous useful discussions.

[1] N. Nücker, H. Romberg, X. X. Xi, J. Fink. B. Gegenheimer, and Z. X. Zhao, Phys. Rev. B **39,** 6619 (1989).
[2] M. E. Garsia and K. H. Bennemann, Phys. Rev. B **40,** 8809 (1989).
[3] R. Liu, B. W. Veal, A. P. Paulikas, J. W. Downey, H. Shi, C. G. Olson, C. Gu, A. I. Arko, and J. J. Joyce, Phys. Rev. B **45,** 5614 (1992).
[4] F. C. Zhang and T. M. Rice, Phys. Rev. B **37,** 3759 (1988).
[5] E. Eskes, G. A. Sawatzky, and L. F. Feiner, Physica C **160,** 424 (1989).
[6] H. Matsukawa, and H. Fukuyama, J. Phys. Soc. Japan **59,** 1723 (1990).
[7] M. V. Eremin, R. Markendorf, and S. V. Varlamov, Solid State Commun. **88,** 15 (1993).
[8] R. P. Gupta and S. K. Sen, Phys. Rev. A **8,** 1169 (1973).
[9] R. R. Sharma, Phys. Rev. B **6,** 4310 (1972).
[10] A. Yu. Zavidonov, M. V. Eremin, O. N. Bakharev, A. V. Egorov, V. V. Tagirov, and M. A. Teplov, Superconductivity (in Russian) 3 **N 8,** 1597 (1990).
[11] H. Yasuoka, T. Shimizu, S. Sasaki, Y. Ueda, and K. Kosuge, Hyperfine Int. **49,** 167 (1989).
[12] K. Schwarz, C. Ambrosch-Draxl, and B. Blaha, Phys. Rev. B **42,** 2051 (1990).
[13] D. J. Singh, K. Schwarz, and P. Blaha, Phys. Rev. B **46,** 5849 (1992).
[14] K. Schwarz, private communication.
[15] O. A. Anikeenok, M. V. Eremin, R. Sh. Zhdanov, V. V. Naletov, M. P. Radionova, and M. A. Teplov, JETP Lett. **54,** 149 (1991).
[16] B. Bucher, P. Steiner, J. Karpinski, E. Kaldis, and P. Wachter, Phys. Rev. Lett. **70,** 2012 (1993).